Deep learning based design of thermal metadevices

Qingxiang Ji, Xueyan Chen, Jun Liang, Guodong Fang, Vincent Laude, Thiwanka Arepolage, Sébastien Euphrasie, Julio Andrés Iglesias Martinez, Sébastien Guenneau, Muamer Kadic

Deep Learning Based Design of Thermal Metadevices

Qingxiang Ji[a], Xueyan Chen[a], Jun Liang[b,*], Guodong Fang [a], Vincent Laude[c], Thiwanka Arepolage [c], Sébastien Euphrasie [c], Julio Andrés Iglesias Martínez [c], Sébastien Guenneau[d], Muamer Kadic[c,*]

[a] *National Key Laboratory of Science and Technology on Advanced Composites in Special Environments, Harbin Institute of Technology, Harbin, 150001, China*

[b] *Institute of Advanced Structure Technology, Beijing Institute of Technology, Beijing 100081, China*

[c] *Institute FEMTO-ST, CNRS, University Bourgogne Franche-Comté, 25000 Besançon, France*

[d] *UMI 2004 Abraham de Moivre-CNRS, Imperial College London, SW7 2AZ, UK*

Abstract

Thermal metadevices obtained from transformation optics have recently attracted wide attention due to their vast potential for thermal management. However, these devices require extreme material parameters that are difficult to achieve in large-scale applications. Here, we design a thermal concentrator using a machine learning method and demonstrate the thermal concentration performance of the designed device. We first define an architecture with a single isotropic material. Deep learning models based on artificial neural networks are implemented to retrieve design geometry parameters ensuring that the required spatially varying anisotropy is achieved. We implement the optimized architecture into a thermal concentrator, fabricate samples and experimentally demonstrate that the designed metamaterial can simultaneously concentrate the heat flux in its core and minimize perturbations to the external thermal field. Our approach paves new avenues for the design of thermal management devices and, more generally, enables feasible solutions for inverse heat manipulation problems.

Keywords: Thermal metadevice; Heat manipulation; Neural network; Optimization; Effective medium

1. Introduction

The effective control or manipulation of heat flow is an evolving research field combining transformation thermodynamics and metamaterials [1, 2, 3, 4, 5, 6, 7, 8, 9, 10, 11, 12, 13, 14, 15, 16, 17, 18, 19, 20, 21, 22, 23, 24]. Following this concept, a class of novel thermal metadevices, i.e. thermal cloaks, concentrators and invisible sensors, have been proposed [25, 26, 27, 28, 29, 30, 31, 32, 33, 34]. Transformation-based thermal metadevices manipulate heat flows through tailored constitutive parameters. However, they face the major challenge of requiring bulk material compositions showing both anisotropy and inhomogeneity. In contrast, it is often desirable in practical applications to retain flexibility in structural design by requiring only materials with realistic physical properties.

Pioneering experimental results on molding heat flows using anisotropic composite structures have been reported [30, 35, 36, 37]. Another promising route is to build bi-layer meta-devices involving bulk isotropic materials by employing the scattering-cancellation method [38, 39, 40, 41, 42, 43]. Such devices can be designed to be homogeneous, but they are generally limited to regular configurations. Researchers have also designed thermal metadevices using topology optimization. These show good performance using regular material compositions [44, 45, 46]. However, the complexity of the obtained configurations adds fabrication difficulties and makes them challenging for real applications. Thermal cloak design methods have further been developed based on inverse problem theory, which re-

[1] liangjun@bit.edu.cn, muamer.kadic@femto-st.fr

moves material anisotropy and is appropriate for irregular shapes [47, 48, 49]. In general, the so-called inverse homogenization theory, which has been developed over the past twenty years to retrieve periodic or random mixtures of materials achieving given effective properties (e.g. conductivity), shows that admissible composites depend notably on the geometry and connectedness of the inclusions within the host medium [50, 51]. For a given effective medium, the challenge is thus to seek feasible structured media within a very large class of composites that would be hard to fabricate in practice. For instance, an inverse homogenization design of an electromagnetic cloak was proposed in reference [52] with isotropic dielectric-magnetic and randomly distributed spheroidal particles with specific orientation achieving the spatially varying anisotropy required by transformation optics.

We note that the transformed material parameters of metadevices can be also approximated by single-material architectures with tailored anisotropy [2, 5, 53, 54]. Hence, the goal becomes to seek a particular configuration such that the required constitutive properties are well mimicked [30, 55, 53]. In this work, we present a general road map to build thermal metadevices based on the optimization of single-material architectures, for ease of fabrication and availability of realistic materials. A deep learning model is employed in the optimization process, resulting in high accuracy and low-cost computation. Such a model can intelligently learn the intrinsic relation linking structural parameters and their influence on thermal concentration from a small-size database. In contrast, conventional optimization methods may get stuck in local minima [56]. In addition, the practical implementation requires flexibility and diversity in design parameters due to the presence of external constraints. These properties are efficiently realized by the deep learning network using probabilistic prediction.

2. Methods and results

2.1. Concept design

Without loss of generality, the thermal concentrating problem is discussed in a 2D framework but it could be readily extended to a 3D framework. Note that the design process is also applicable to other metadevices such as invisibility cloaks. Indeed, the approach can be applied to any transformation based medium, and is not restricted to thermal problems.

Let us assume that we want to create a cylindrical thermal concentrator with inner radius $r_1 = 0.01$ m and outer radius $r_2 = 0.04$ m. In our design, the thermal conductivity of the background is $k_b = 132\,\mathrm{W}\cdot\mathrm{m}^{-1}\cdot\mathrm{K}^{-1}$. Following transformation physics [2, 5, 54], radial and tangential heat conductivities for the shell region are obtained as $k'_r = 264\,\mathrm{W}\cdot\mathrm{m}^{-1}\cdot\mathrm{K}^{-1}$ and $k'_\theta = 66\,\mathrm{W}\cdot\mathrm{m}^{-1}\cdot\mathrm{K}^{-1}$, respectively. Their practical implementation demands simple-material structures that exhibit prescribed anisotropic effective-medium properties, which can be further realized by artificial architectures with optimized geometry parameters.

A single-composition (i.e., copper) architecture is proposed with four dimensionless design parameters (see Fig. 1). Now we turn to realize the shell region properties by tailoring the anisotropy of the proposed architectures, that is, to find the particular design parameters that best mimic the transformed medium. The optimization problem amounts to minimizing the objective function:

$$E(k_1, k_2; \alpha, \beta) = \alpha \left|k_1 - k'_\theta\right| + \beta \left|k_2 - k'_r\right|, \qquad (1)$$

where α and β are weighting factors for the two objective sub-functions such that $\alpha + \beta = 1$, k_1 and k_2 denote the thermal conductivity of the homogenized unit cell in directions 1 and 2, respectively (see the insets in Fig. 1). We select $\alpha = \beta = 0.5$, i.e. equal weights for the diagonal tensor elements k_1 and k_2. The function $E(k_1, k_2; \alpha, \beta)$ measures the overall difference between obtained and objective values. This function reveals how well the effective properties of the established architecture mimic the transformed medium. Ideal parameters achieve zero $E(k_1, k_2; \alpha, \beta)$.

2.2. Forward-modeling network

We propose a forward-modeling network to accurately predict the effective thermal conductivity for given design parameters (see also Fig. S1 in the supplementary information). The forward model builds a fully connected network between the design space $D = [d_1, d_2, d_3, d_4]$ as the input layer and the result

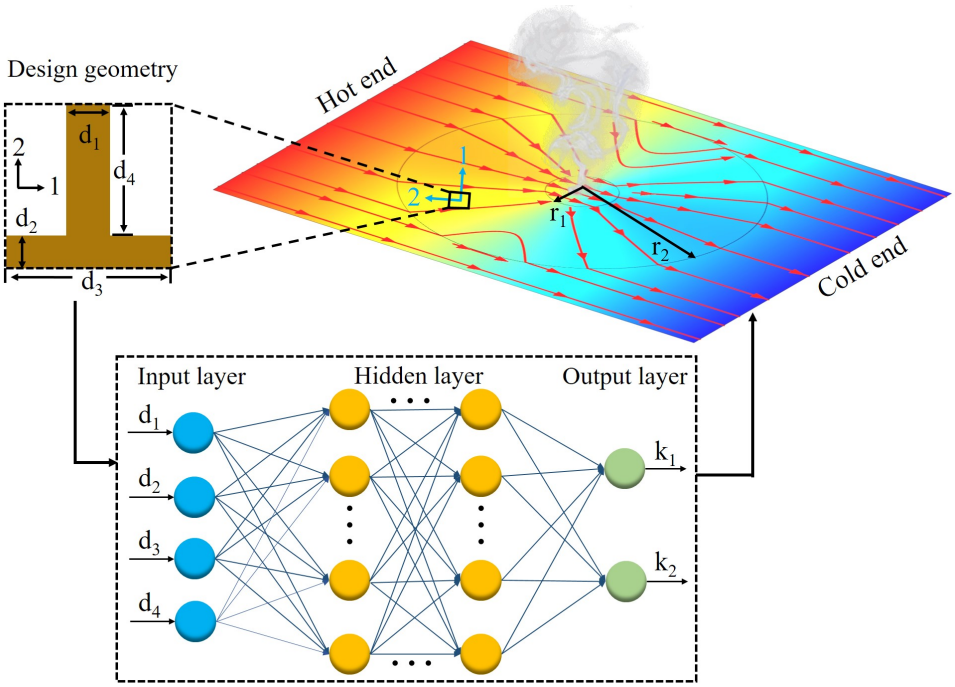

Fig. 1. Schematic diagram representation of the design problem. A single-material structure is designed and optimized by an artificial neural network. We implement the optimized design geometry into the thermal concentrator extending in the shell region $r_1 < r < r_2$ and realize the desired thermal concentration effect.

space $R = [k_1, k_2]$ as the output layer, as shown in Fig. 1. For the analysis, we generate a database containing 1000 data samples for training, 200 data samples for validation, and 300 data samples for final testing. Each data sample is represented by four design parameters and two output parameters. The training data set is used to train the network by optimizing the neural network weights, while the validation data serves for checking and avoiding overfitting, and the testing data examines the prediction accuracy of the network. We apply the optimal Latin hypercube sampling technique to obtain the original sample control points. This process is conducted to create sample points that spread as evenly as possible within design space: this will increase prediction accuracy and efficiency. After initial estimation, we define ranges of the design parameters as $0.5 < d_1 < 0.8$, $0.05 < d_2 < 0.2$, $0.8 < d_3 < 1.2$, $0.8 < d_4 < 1.2$. We mention at this point that broader ranges may decrease the prediction efficiency, but can be compensated for by building more data samples. Furthermore, the architecture is designed at the macro-scale. If distances d_i were considered at the micro/nano-scale, heat flow could change from diffusive transport to wave (coherent phonon) transport. In such case, the proposed method may not be applicable [57].

Data obtained from the optimal Latin hypercube sampling technique are normalized to expedite convergence of the network. Then these data are fed into the network, where the neural network weights are continuously optimized to accelerate convergence of the algorithm. The mean square error $\frac{1}{n}\sum_1^n(\hat{E}-E)^2$ is used to represent the loss function between the normalized and desired output, where $\hat{E}$ and E respectively denote the predicted values and real values. The learning curves for training, validation and testing data are shown in Fig. 2a as a function of training epochs. All three errors drop sharply as training proceeds, until convergence is gradually obtained after 400 epochs, implying completion of the training phase. Errors are small and are evenly distributed, suggesting a smooth network without over-fitting issues. Due to the unique one-to-one mapping between design space and response in the forward problem, the training process converges straightforwardly.

To check the prediction accuracy of the trained model, we evaluate it on a group of 200 new data

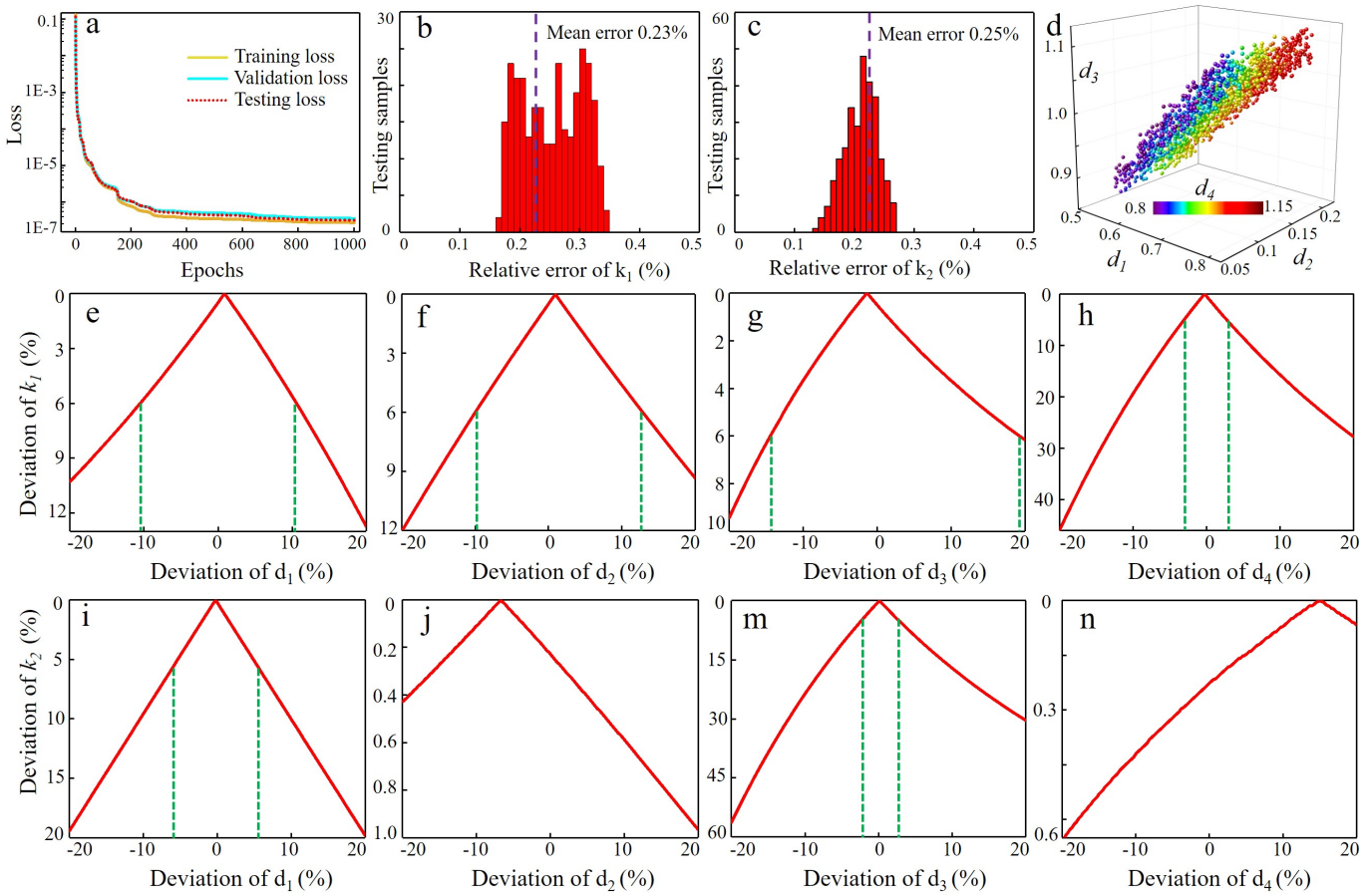

Fig. 2. Forward network learning process and results. (a) The learning curves for training, validation and data testing are shown as a function of the training epochs. (b,c) Histogram of relative errors for the testing samples. The mean errors are indicated by purple dashed lines. (d) Latent design space and (e-n) sensitivity of the effective conductivity to constructed parameters. The green dashed lines mark the deviation ranges within which the built architecture will exhibit effective properties differing by less than 6% compared with the target values.

samples that are not used in the training process. We compare the results predicted by the trained network and those from finite element analysis (FEA). The mean relative errors are reported in Fig. 2b, c, where we observe that the mean relative errors all fall into the range $0-0.5\%$ while the mean errors are less than 0.25%. Since the results demonstrate extremely high prediction accuracy of the proposed network (over 99.5%), we can safely conclude that the pretrained network is credible in this scenario.

2.3. Determination of optimal design parameters

Practical applications often require feasible design parameters of the architecture to exhibit required thermal properties. Using the established forward network, we generate 10000 new sets of data samples within the prescribed range. Note that the 10000 new samples are created from the neural network directly for optimization, while the original 1500 samples are calculated by finite element analysis as a database. Consequently, we filter out the optimal design parameters that lead to output results closest to the target values within the 10000 new samples (see Fig. S2 in the supplementary information). Optimal parameters are obtained as $d_1 = 0.5364$, $d_2 = 0.136$, $d_3 = 0.9028$ and $d_4 = 0.9186$. We calculate thermal conductivities of the optimized architecture and compare them with the target values in Tab. 1. It is seen that the obtained parameters closely mimic those of the desired transformed medium, thus validating the prediction efficiency.

2.4. Probabilistic design space

We have obtained one precise set of optimal design parameters that generates the required thermal conductivity, yet practical implementation demands diversity in design parameters due to the possible unavailability of manufacture and deviations from the desired design parameters. It is essential to enhance the generalization and robustness of the neural network by introducing probabilistic prediction of the design parameters. Here, the latent space concept is adopted for probabilistic representation [58]. Therefore, 1600 sets of design parameters are generated through the network established before, forming the design space. We plot distributions of the design space with the criterion of maximum deviation by 6% (from the target values) in Fig. 2d. Architectures built using these parameters will exhibit effective thermal conductivity differing by less than 6% from target values. Such probabilistic design space reveals the sensitivity of the device's parameters on effective properties, hence further allowing for more diversity and flexibility in the design and fabrication of thermal meta-devices.

To give more details on the latent space, we plot the sensitivity of the effective conductivity to constructed parameters in Fig. 2(e-n). We show the deviation range of each parameter that will exhibit effective properties differing by less than 6% from target values. As expected, we observe a significant influence of parameter d_4 on k_1, and a significant influence of parameter d_3 on k_2. In Fig. 2j,n nearly null sensitivity is observed, since the conductivity changes by less than 1% even though parameter d_2 (or d_4) changes by 20%. Also note in Fig. 2(e-n) that optimized parameters slightly deviate from ideal ones. This corresponds to the fact that the obtained effective conductivity values differ slightly from target values. We stress that this difference is negligible, and can be improved by generating more data samples in the filtering process.

Table 1
Comparison of predicted and target values for the derived set of parameters.

	Predicted	Targeted	Difference
$k_1(\mathrm{Wm^{-1}K^{-1}})$	65.7	66	0.4%
$k_2(\mathrm{Wm^{-1}K^{-1}})$	264.6	264	0.2%

3. Transformed couplet heat equation

After integrating the heat equation with respect to the z variable and combining with the top and bottom surface boundary conditions (convection and radiation), the problem is expressed in two dimensions (x, y) as:

$$\nabla\cdot(k\nabla T)-\rho c\frac{\partial T}{\partial t}-P\left[h\left(T-T_a\right)+\varepsilon\left(T^4-T_a^4\right)\right]=0, \tag{2}$$

where T_a is the ambient temperature, h represents the convection coefficient and ε denotes surface emissivity. $P = 2/\delta$ where δ is the thickness. In principle all terms of the governing equation should be transformed, namely, not only the conductivity (as very often reported) but also the emission and the convective terms. We shall consider the convective term to include a Jacobian $\det(J)$ when applying a coordinate change in Eq. (2). The nonlinear term $\varepsilon\left(T^4 - T_a^4\right)$, however, is not suitable for direct transformation, but fortunately it has relatively small influence for low temperature differences [59].

Consider the coordinate transformation from original space $(x,\ y,\ z)$ to physical space $(x',\ y',\ z')$, the transformed heat governing equation without emissive terms takes the form

$$\nabla\cdot\left(k'\nabla T\right)-\rho' c'\frac{\partial T}{\partial t}-Ph'\left(T-T_a\right)=0, \tag{3}$$

where the transformed parameters satisfy

$$k'=\frac{JKJ^T}{\det(J)},\ (\rho c)'=\frac{\rho c}{\det(J)},\ h'=\frac{h}{\det(J)}\ , \tag{4}$$

with $J = \partial(x', y', z')/\partial(x, y, z)$ the Jacobian matrix and J^T its transpose.

If we neglect convection and radiation, as is often assumed in the literature, Eq. (3) simplifies to

$$\nabla\cdot\left(k'\nabla T\right)-\rho' c'\frac{\partial T}{\partial t}=0. \tag{5}$$

Fig. 3 shows the simulation results obtained when considering the different contributions (plate thickness 2 mm and ambient temperature 293 K). The results in Fig. 3c,d show that the convective term

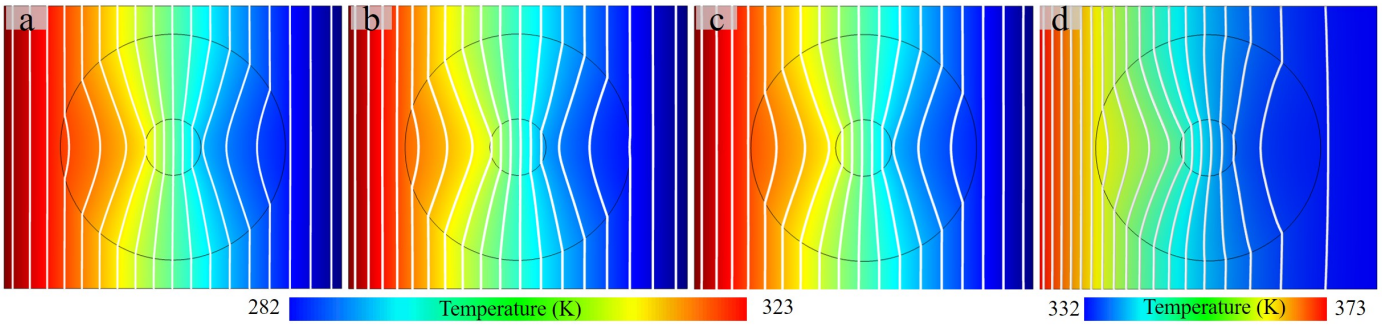

Fig. 3. Temperature fields: (a) without convection, obtained from Eq. (5); (b) with transformed convective terms, obtained from Eq. (3); (c-d) with convective terms ($h = 15\ \mathrm{W \cdot m^{-2} \cdot K^{-1}}$), obtained from Eq. (2).

deteriorates concentration especially for high temperatures, for which the external temperature profile is disturbed. However, thermal metadevices including the transformed convective term show good thermal neutrality in Fig. 3b (see also Fig. S3 in the supplementary information). Actually, though heat is expected to diffuse along the plate, heat radiation and convection to the ambient air seem more or less unavoidable. Heat dissipation via convection and radiation decrease the amount of heat that is transported via conduction along the plate, which is detrimental to thermal neutrality. We note in passing that the transformation theory for thermal convection and manipulation of heat fluid flow can be physically implemented with anisotropic porous media, though this is beyond our considerations [60, 61]. The relevant homogenization literature includes e.g Ref. [62].

4. Experimental validation

We have fabricated the proposed thermal concentrator with copper and characterized such a device that molds the flow of heat. The background thermal conductivity $k_b = 132\ \mathrm{W \cdot m^{-1} \cdot K^{-1}}$ is not readily available in naturally existing materials. We achieve it by drilling holes into the copper plate (thermal conductivity $k_c = 394\ \mathrm{W \cdot m^{-1} \cdot K^{-1}}$), and the holes are filled with air in the room temperature (thermal conductivity $k_a = 0.026\ \mathrm{W \cdot m^{-1} \cdot K^{-1}}$). According to Maxwell-Garnett theory [63, 64], the effective conductivity is $k_b = k_c\left[1 + \frac{2(k_a-k_c)f}{k_a+k_c-(k_a-k_c)f}\right]$, where f denotes the fraction area of holes. Following this approach, we obtain $f = 0.5$ and thus introduce an array of holes (diameter 1.6 mm) in the plate with equal spacing 2 mm.

A photograph of the experimental system is shown in Fig. 4a, where local heating on the left side of the plate is realized by a tank filled with hot water whereas the right side is immersed in an identical tank filled with water at room temperature. The other sides are left free. An elevator is used to adjust the position of the infrared camera to capture images of the temperature profiles. The CNC machining technique is used to produce the pattern shown in Fig. 4a. Note that increasing the number of layers and sectors, one can accurately approximate the idealized thermal concentrator parameters. However, a large number of layers will increase the fabrication complexity. Considering the trade-off between performance and easiness of fabrication, we have made a thermal concentrator with 5 radial layers and 25 tangential sectors (see Fig. 4a).

To measure the temperature profiles via Planck thermal emission, we used an infrared thermal camera (FLIR A6702sc) to capture thermal images. Considering that copper is highly reflective, we cover the sample with acrylic paint to reduce the surface reflectivity and with insulating tape to facilitate the capture of images. The thermal conductivity of acrylic is around $0.2\ \mathrm{W \cdot m^{-1} \cdot K^{-1}}$ and is 4 orders of magnitude smaller than the thermal conductivity of copper, thus hardly influencing the heat diffusion process. Numerical and experimental results are shown in Fig. 4b,c. We observe that the proposed device successfully fulfills its tasks in that heat flux is focused to the central region and that simultaneously the thermal field remains unaffected outside the device. The

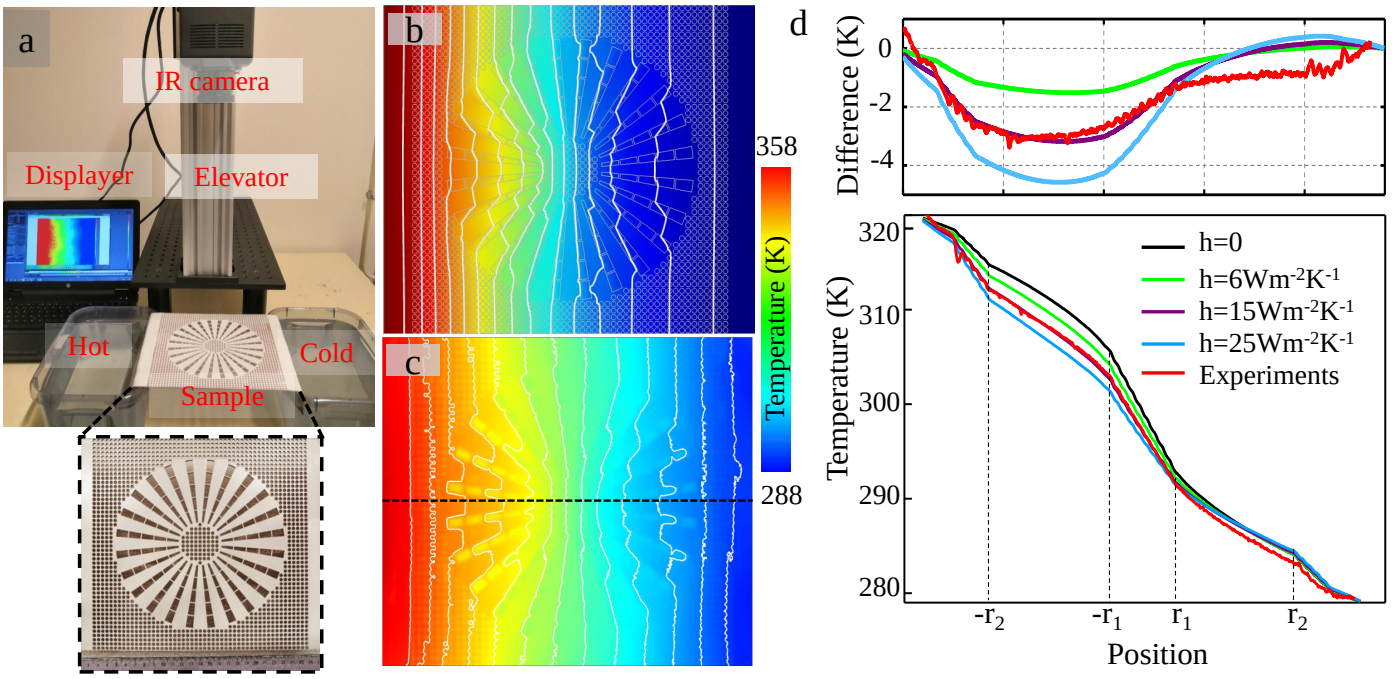

Fig. 4. (a) Photograph of the experimental system. (b) Simulated and (c) measured temperature distributions. The white lines denote temperature iso-lines and the black line denotes the observation line. (d) Bottom: temperature along the observation line considering different thermal convection coefficients. Top: temperature difference between the convective case and the zero-convection case.

heat density is larger in the inner domain than in its surroundings. Furthermore, the temperature field outside the device is almost not affected. The experimental results are consistent with numerical calculations, validating the design. Note that experimental results show a better agreement with numerical simulation considering that the thermal convection coefficient $h = 15\ \mathrm{W} \cdot \mathrm{m}^{-2} \cdot \mathrm{K}^{-1}$. The larger the thermal convection coefficient, the worse the thermal concentration effect.

5. Conclusion

Summarizing, we have demonstrated the machine learning driven design of a thermal concentrator through the optimization of single-material architectures. An artificial neural network is proposed to accurately predict the effective material property for given design geometry parameters. Optimal design parameters are then retrieved for target thermal conductivities. The probabilistic space of the design parameters is used to reveal the sensitivity of the design parameters to the effective conductivity and the generation of desired results with miscellaneous design.

We implement a thermal concentrator based on the optimized architectures and fabricate a sample by the CNC machining technique. Both numerical simulations and experimental results show good thermal concentration. We emphasize that the approach can be used to automate the design process with more complex architectures, offering a non-unique solution space. Finally, our approach would work equally well for other diffusion (e.g. mass, matter) or wave (acoustic, electromagnetic, elastodynamic, hydrodynamic) fields governed by linear partial differential equations.

Declaration of Competing Interest

The authors declare that they have no known competing financial interests or personal relationships that could have appeared to influence the work reported in this paper.

Acknowledgments

We thank Vincent Pêcheur, Mathieu Chauvet and Thibaut Sylvestre for help with the infrared camera. This work was supported by the EIPHI Graduate School [grant number ANR-17-EURE-0002]; the

French Investissements d'Avenir program, project ISITEBFC [grant number ANR-15-IDEX-03]; and the National Natural Science Foundation of China [grant numbers Nos. 11732002 and 12090034]. We are also grateful to Natural Science Foundation of Heilongjiang Province of China (Grant Nos. YQ2021A004).

References

[1] A. Greenleaf, M. Lassas, G. Uhlmann, Anisotropic conductivities that cannot be detected by eit, Physiological measurement 24 (2) (2003) 413.

[2] J. B. Pendry, D. Schurig, D. R. Smith, Controlling electromagnetic fields, Science 312 (5781) (2006) 1780–1782.

[3] U. Leonhardt, Optical conformal mapping, science 312 (5781) (2006) 1777–1780.

[4] C. Fan, Y. Gao, J. Huang, Shaped graded materials with an apparent negative thermal conductivity, Applied Physics Letters 92 (25) (2008) 251907.

[5] S. Guenneau, C. Amra, D. Veynante, Transformation thermodynamics: cloaking and concentrating heat flux, Optics Express 20 (7) (2012) 8207–8218.

[6] M. Kadic, S. Guenneau, S. Enoch, S. A. Ramakrishna, Plasmonic space folding: Focusing surface plasmons via negative refraction in complementary media, ACS nano 5 (9) (2011) 6819–6825.

[7] R. Schittny, M. Kadic, T. Bückmann, M. Wegener, Invisibility cloaking in a diffusive light scattering medium, Science 345 (6195) (2014) 427–429.

[8] M. Kadic, T. Bückmann, R. Schittny, M. Wegener, Experiments on cloaking in optics, thermodynamics and mechanics, Philosophical Transactions of the Royal Society A: Mathematical, Physical and Engineering Sciences 373 (2049) (2015) 20140357.

[9] R. Schittny, A. Niemeyer, M. Kadic, T. Bückmann, A. Naber, M. Wegener, Transient behavior of invisibility cloaks for diffusive light propagation, Optica 2 (2) (2015) 84–87.

[10] R. Schittny, A. Niemeyer, F. Mayer, A. Naber, M. Kadic, M. Wegener, Invisibility cloaking in light-scattering media, Laser & Photonics Reviews 10 (3) (2016) 382–408.

[11] A. Alwakil, M. Zerrad, M. Bellieud, C. Amra, Inverse heat mimicking of given objects, Scientific Reports 7 (1) (2017) 1–17.

[12] M. Kadic, G. W. Milton, M. van Hecke, M. Wegener, 3d metamaterials, Nature Reviews Physics 1 (3) (2019) 198–210.

[13] M. McCall, J. B. Pendry, V. Galdi, Y. Lai, S. Horsley, J. Li, J. Zhu, R. C. Mitchell-Thomas, O. Quevedo-Teruel, P. Tassin, et al., Roadmap on transformation optics, Journal of Optics 20 (6) (2018) 063001.

[14] R. V. Craster, S. Guenneau, H. Hutridurga, G. A. Pavliotis, Cloaking via mapping for the heat equation, Multiscale Modeling & Simulation 16 (3) (2018) 1146–1174.

[15] S. Yang, J. Wang, G. Dai, F. Yang, J. Huang, Controlling macroscopic heat transfer with thermal metamaterials: theory, experiment and application, Physics Reports 908 (2021) 1–65.

[16] J. Huang, Theoretical Thermotics, Springer, 2020.

[17] Q. Gao, J. Ai, S. Tang, M. Li, Y. Chen, J. Huang, H. Tong, L. Xu, L. Xu, H. Tanaka, et al., Fast crystal growth at ultra-low temperatures, Nature Materials 20 (10) (2021) 1431–1439.

[18] Z. Zhou, X. Shen, C. Fang, J. Huang, Programmable thermal metamaterials based on optomechanical systems, ES Energy & Environment 6 (3) (2019) 85–91.

[19] J.-P. Huang, Thermal metamaterials make it possible to control the flow of heat at will-2, ES Energy & Environment 7 (2) (2020) 1–3.

[20] L. Xu, S. Yang, G. Dai, J. Huang, Transformation omnithermotics: simultaneous manipulation of three basic modes of heat transfer, ES Energy & Environment 7 (7) (2020) 65–70.

[21] Y. Xiao, Q. Hao, Nanoslot patterns for enhanced thermal anisotropy of si thin films, International Journal of Heat and Mass Transfer 170 (2021) 120944.

[22] Q. Hao, Y. Xiao, Periodic nanoslot patterns as an effective approach to improving the thermoelectric performance of thin films, Physical Review Applied 13 (6) (2020) 064020.

[23] Y. Li, W. Li, T. Han, X. Zheng, J. Li, B. Li, S. Fan, C. W. Qiu, Transforming heat transfer with thermal metamaterials and devices, Nature Reviews Materials 6 (6) (2021) 488–507.

[24] J. Guo, G. Xu, D. Tian, Z. Qu, C. W. Qiu, Passive ultraconductive thermal metamaterials, Advanced Materials (2022) 2200329.

[25] M. Farhat, S. Guenneau, S. Enoch, Ultrabroadband elastic cloaking in thin plates, Physical Review Letters 103 (2) (2009) 024301.

[26] T. Yang, X. Bai, D. Gao, L. Wu, B. Li, J. T. Thong, C. W. Qiu, Invisible sensors: Simultaneous sensing and camouflaging in multiphysical fields, Advanced Materials 27 (47) (2015) 7752–7758.

[27] R. Hu, S. Zhou, Y. Li, D.-Y. Lei, X. Luo, C. W. Qiu, Illusion thermotics, Advanced Materials 30 (22) (2018) 1707237.

[28] X. Shen, J. Huang, Thermally hiding an object inside a cloak with feeling, International Journal of Heat and Mass Transfer 78 (2014) 1–6.

[29] J. Qin, W. Luo, P. Yang, B. Wang, T. Deng, T. Han, Experimental demonstration of irregular thermal carpet cloaks with natural bulk material, International Journal of Heat and Mass Transfer 141 (2019) 487–490.

[30] R. Schittny, M. Kadic, S. Guenneau, M. Wegener, Experiments on transformation thermodynamics: molding the flow of heat, Physical Review Letters 110 (19) (2013) 195901.

[31] S. Huang, J. Zhang, M. Wang, R. Hu, X. Luo, Macroscale thermal diode-like black box with high transient rectifica-

tion ratio, ES Energy & Environment 6 (2019) 51–6.
[32] P. Jin, L. Xu, T. Jiang, L. Zhang, J. Huang, Making thermal sensors accurate and invisible with an anisotropic monolayer scheme, International Journal of Heat and Mass Transfer 163 (2020) 120437.
[33] P. Jin, S. Yang, L. Xu, G. Dai, J. Huang, X. Ouyang, Particle swarm optimization for realizing bilayer thermal sensors with bulk isotropic materials, International Journal of Heat and Mass Transfer 172 (2021) 121177.
[34] Y. Li, J. Xi, C. K. W. Leung, T. Li, W. Y. Tam, J. Li, Imaging by unsupervised feature learning of the wave equation, Physical Review Applied 16 (6) (2021) 064039.
[35] S. Narayana, Y. Sato, Heat flux manipulation with engineered thermal materials, Physical Review Letters 108 (21) (2012) 214303.
[36] J. Li, Y. Li, T. Li, W. Wang, L. Li, C. W. Qiu, Doublet thermal metadevice, Physical Review Applied 11 (4) (2019) 044021.
[37] B. Tian, J. Wang, G. Dai, X. Ouyang, J. Huang, Thermal metadevices with geometrically anisotropic heterogeneous composites, International Journal of Heat and Mass Transfer 174 (2021) 121312.
[38] T. Han, X. Bai, D. Gao, J. T. Thong, B. Li, C. W. Qiu, Experimental demonstration of a bilayer thermal cloak, Physical Review Letters 112 (5) (2014) 054302.
[39] M. Farhat, P.-Y. Chen, H. Bagci, C. Amra, S. Guenneau, A. Alu, Thermal invisibility based on scattering cancellation and mantle cloaking, Scientific reports 5 (1) (2015) 1–9.
[40] X. Zhang, X. He, L. Wu, Ellipsoidal bifunctional thermal-electric transparent device, Composite Structures 234 (2020) 111717.
[41] H. Xu, X. Shi, F. Gao, H. Sun, B. Zhang, Ultrathin three-dimensional thermal cloak, Physical Review Letters 112 (5) (2014) 054301.
[42] G. Xu, X. Zhou, J. Zhang, Bilayer thermal harvesters for concentrating temperature distribution, International Journal of Heat and Mass Transfer 142 (2019) 118434.
[43] M. Farhat, S. Guenneau, P.-Y. Chen, A. Alù, K. N. Salama, Scattering cancellation-based cloaking for the maxwell-cattaneo heat waves, Physical Review Applied 11 (4) (2019) 044089.
[44] G. V. Alekseev, D. A. Tereshko, Particle swarm optimization-based algorithms for solving inverse problems of designing thermal cloaking and shielding devices, International Journal of Heat and Mass Transfer 135 (2019) 1269–1277.
[45] G. Fujii, Y. Akimoto, Topology-optimized thermal carpet cloak expressed by an immersed-boundary level-set method via a covariance matrix adaptation evolution strategy, International Journal of Heat and Mass Transfer 137 (2019) 1312–1322.
[46] G. Fujii, Y. Akimoto, Cloaking a concentrator in thermal conduction via topology optimization, International Journal of Heat and Mass Transfer 159 (2020) 120082.
[47] J. Guo, Z. Qu, Thermal cloak with adaptive heat source to proactively manipulate temperature field in heat conduction process, International Journal of Heat and Mass Transfer 127 (2018) 1212–1222.
[48] J. Guo, Z. Qu, X. Wang, A reverse thermal cloak design method based on inverse problem theory, ES Energy & Environment 7 (3) (2020) 71–83.
[49] Y. Xiao, Q. Chen, Q. Hao, Inverse thermal design of nanoporous thin films for thermal cloaking, Materials Today Physics 21 (2021) 100477.
[50] D. Łydżba, A. Różański, I. Sevostianov, D. Stefaniuk, Principle of equivalent microstructure in micromechanics and its connection with the replacement relations. thermal conductivity problem, International Journal of Engineering Science 144 (2019) 103126.
[51] C. Orum, E. Cherkaev, K. M. Golden, Recovery of inclusion separations in strongly heterogeneous composites from effective property measurements, Proceedings of the Royal Society A: Mathematical, Physical and Engineering Sciences 468 (2139) (2012) 784–809.
[52] T. H. Anderson, T. G. Mackay, A. Lakhtakia, Toward a cylindrical cloak via inverse homogenization, JOSA A 29 (3) (2012) 239–243.
[53] Q. Ji, X. Chen, J. Liang, V. Laude, S. Guenneau, G. Fang, M. Kadic, Designing thermal energy harvesting devices with natural materials through optimized microstructures, International Journal of Heat and Mass Transfer 169 (2021) 120948.
[54] T. Han, J. Zhao, T. Yuan, D. Y. Lei, B. Li, C. W. Qiu, Theoretical realization of an ultra-efficient thermal-energy harvesting cell made of natural materials, Energy & Environmental Science 6 (12) (2013) 3537–3541.
[55] L. Pomot, C. Payan, M. Remillieux, S. Guenneau, Acoustic cloaking: Geometric transform, homogenization and a genetic algorithm, Wave Motion 92 (2020) 102413.
[56] H. Gao, Y.-f. Zhu, X.-d. Fan, B. Liang, J. Yang, J.-C. Cheng, Non-blind acoustic invisibility by dual layers of homogeneous single-negative media, Scientific reports 7 (1) (2017) 1–7.
[57] M. Maldovan, Narrow low-frequency spectrum and heat management by thermocrystals, Physical review letters 110 (2) (2013) 025902.
[58] W. W. Ahmed, M. Farhat, X. Zhang, Y. Wu, Deterministic and probabilistic deep learning models for inverse design of broadband acoustic cloak, Physical Review Research 3 (1) (2021) 013142.
[59] L. Xu, J. Huang, Metamaterials for manipulating thermal radiation: transparency, cloak, and expander, Physical Review Applied 12 (4) (2019) 044048.
[60] Y. A. Urzhumov, D. R. Smith, Fluid flow control with transformation media, Physical review letters 107 (7) (2011) 074501.
[61] G. Dai, J. Huang, A transient regime for transforming thermal convection: Cloaking, concentrating, and rotating creeping flow and heat flux, Journal of Applied Physics 124 (23) (2018) 235103.
[62] N. Murphy, E. Cherkaev, J. Zhu, J. Xin, K. Golden, Spec-

tral analysis and computation for homogenization of advection diffusion processes in steady flows, Journal of Mathematical Physics 61 (1) (2020) 013102.

[63] D. Bigoni, S. Serkov, M. Valentini, A. Movchan, Asymptotic models of dilute composites with imperfectly bonded inclusions, International journal of solids and structures 35 (24) (1998) 3239–3258.

[64] G. W. Milton, S. K. Serkov, Neutral coated inclusions in conductivity and anti–plane elasticity, Proceedings of the Royal Society of London. Series A: Mathematical, Physical and Engineering Sciences 457 (2012) (2001) 1973–1997.